Published in final edited form as:
Cytoskeleton (Hoboken). 2013 May ; 70(5): 281–295. doi:10.1002/cm.21110.

Biochemical and bioinformatic analysis of the MYO19 motor domain

Rebecca C. Adikes[3,4], **William C. Unrath**[2], **Christopher M. Yengo**[2], and **Omar A. Quintero**[1,2,3,*]

[1]Department of Biology, University of Richmond, VA 23173

[2]Department of Cellular and Molecular Physiology, Penn State College of Medicine, Hershey, PA 17033

[3]Program in Biochemistry, Mount Holyoke College, South Hadley, MA 01075

[4]Biological and Biomedical Sciences Program, University of North Carolina, Chapel Hill, NC 27599

Abstract

Mitochondrial dynamics are dependent on both the microtubule and actin cytoskeletal systems. Evidence for the involvement of myosin motors has been described in many systems, and until recently a candidate mitochondrial transport motor had not been described in vertebrates. Myosin-XIX (MYO19) was predicted to represent a novel class of myosin and had previously been shown to bind to mitochondria and increase mitochondrial network dynamics when ectopically expressed. Our analyses comparing ∼40 MYO19 orthologs to ∼2000 other myosin motor domain sequences identified instances of homology well-conserved within class XIX myosins that were not found in other myosin classes, suggesting MYO19-specific mechanochemistry. Steady-state biochemical analyses of the MYO19 motor domain indicate that Homo sapiens MYO19 is a functional motor. Insect cell-expressed constructs bound calmodulin as a light chain at the predicted stoichiometry and displayed actin-activated ATPase activity. MYO19 constructs demonstrated high actin affinity in the presence of ATP in actin-cosedimentation assays, and translocated actin filaments in gliding assays. Expression of GFP-MYO19 containing a mutation impairing ATPase activity did not enhance mitochondrial network dynamics, as occurs with wild-type MYO19, indicating that myosin motor activity is required for mitochondrial motility. The measured biochemical properties of MYO19 suggest it is a high-duty ratio motor that could serve to transport mitochondria or anchor mitochondria, depending upon the cellular microenvironment.

Key words/phrases

actin-based motility; myosin biochemistry; mitochondrial dynamics; ATPase; sequence analysis

Introduction

Like many intracellular components, mitochondria undergo dynamic organization mediated through the cytoskeleton. These essential organelles play a central role in metabolism,

*Corresponding author: Omar A. Quintero, Department of Biology, University of Richmond, 28 Westhampton Way, Richmond, VA 23173, Office: (804) 287-6892, Lab: (804) 289-1706, FAX (804) 289-8233, oquinter@richmond.edu.

Author contributions: Hypotheses and experiments in this study were conceived by RCA and OAQ. Experiments were performed by RCA, WCU, CMY, and OAQ. Data were analyzed by RCA, CMY, and OAQ. The manuscript was written by RCA, CMY, and OAQ. Material support provided by CMY and OAQ.

participate in calcium signaling, and are also involved in apoptotic processes. Mitochondrial membrane fission [De Vos et al., 2005; Korobova et al., 2013], mtDNA copy number [Reyes et al., 2011], and intracellular position [Boldogh et al., 2001; Minin et al., 2006] have been shown to require cytoskeletal elements in a variety of systems. A recent study by DuBoff et al. [DuBoff et al., 2012] demonstrated a linkage between the actin and microtubule cytoskeleton in mitochondrial fission in neurons. Additionally, long-distance mitochondrial movement is dependent on microtubule-based motors [Hollenbeck and Saxton, 2005; Morris and Hollenbeck, 1995] whereas short-range movement and docking of mitochondria is achieved via the actin cytoskeleton [Chada and Hollenbeck, 2004; Pathak et al., 2010; Quintero et al., 2009].

Mechanisms for regulating mitochondrial positioning via the actin cytoskeleton vary [Boldogh and Pon 2006]. In yeast, the class V myosin motor, Myo2p, and its light chain, Mlc1p, have been shown to play a direct role in mitochondrial motility and inheritance [Altmann et al., 2008]. *C. elegans* ANC-1 contains an actin binding domain and a nuclear envelope localization domain; mutations in *anc-1* disrupt the positioning and the shape of mitochondria [Starr and Han, 2002]. In *Drosophila* neuronal cells myosin V and VI have been reported to oppose long range microtubule-based movements and facilitate docking of the organelle [Pathak et al., 2010]. In mammalian cell culture, myosin XIX (MYO19) has been shown to play a role in mitochondrial positioning [Quintero et al., 2009].

Although well characterized for their roles as molecular motors, some actomyosin systems are involved in other processes besides transport. Class I myosins bind cellular membranes and have been shown to be involved in the formation of membrane compartments at the plasma membrane as well as the fusion of compartments to the plasma membrane (reviewed in [McConnell and Tyska 2010]). Other roles include the establishing and maintaining membrane tension in a variety of cellular structures [Self et al., 1998; Self et al., 1999; Tyska et al. 2005]. Myosin-membrane interactions underlie long-term potentiation and long term depression, where interactions between class V myosins and the endoplasmic reticulum establish the receptor-content within a dendritic spine, thereby modulating the strength and sensitivity of the synapse [Dekker-Ohno et al., 1996; Lisé et al., 2006; Miyata et al., 2000; Wang et al., 2008].

All myosins have a common actin-activated ATPase motor domain which generates force through conformational changes coupled to biochemical transitions of the ATPase cycle. This motor domain has structural and sequence homology that is conserved throughout the myosin family. However, analysis of the kinetics, structure, and function of different myosins suggest that despite having a common core motor domain, each myosin has differences that tune its chemomechanical activity for specific physiological functions [De La Cruz and Ostap, 2004]. This tuning can be observed as differences in enzymatic and biophysical properties across myosin classes. Specific differences in the amino acid sequence ultimately impact both structure and function [reviewed in Cope et al., 1996; Mooseker and Foth, 2008].

Therefore, insight into the function of uncharacterized myosins can come from comparison to the well-characterized myosins which have known amino acid sequences, structures, and enzymatic properties. The number of available myosin sequences has increased as a result of many large-scale genome sequencing projects, as has the available structural data, and kinetic data. We can now begin to approach the characterization of unknown myosins through a combination of both informatic and experimental approaches.

MYO19 is a novel unconventional myosin which colocalizes with mitochondria and may play an important role in mitochondrial positioning [Quintero et al., 2009]. The aim of this

study was to employ comparative and experimental approaches to further our understanding of the chemomechanical activity of MYO19 by identifying class XIX-specific differences conserved across MYO19 orthologs, and determining the steady-state enzymatic characteristics of the human MYO19 motor domain. Understanding the unique structural components and kinetics of MYO19 will give us insight into its cellular and biological function. Our results indicate that MYO19 is indeed an actin-activated ATPase with the ability to power the translocation of actin filaments *in vitro*, and that motor ATPase activity is required for transporting mitochondria within cells.

Results and Discussion

Sequence analysis reveals conserved variation within class XIX myosins

As reported previously, the human MYO19 gene encodes for a 970 amino acid protein consisting of a motor domain, neck region containing 3 IQ-motifs, and a MYO19-specific mitochondria outer membrane association (MyMOMA) domain [Quintero et al., 2009]. Comparison of alignments of MYO19 orthologs (Figure 1A, Supplemental Figure 1), alignments of human MYO19 to other myosin classes (Supplemental Figure 2), and structural predictions via threading [Combet et al., 2002; Kelley and Sternberg, 2009] allow for the identification of sequences conserved within the core motor domain of MYO19 (Supplemental Figure 3). Analysis of these conserved regions revealed class-specific differences in the core sequences, as well as class-specific insertions that do not appear in other myosins.

The myosin motor contains a Walker-A ATPase domain composed of residues that coordinate ATP and Mg^{2+} in the active site. Catalytic residues mediate the hydrolysis of the β-γ phosphate bond which is followed by release of hydrolysis products. Nucleotide state is communicated to the actin binding region and the lever arm [Cope et al., 1996; Holmes, 2008]. The human MYO19 motor domain contains conserved motifs responsible for coordinating the phosphates of the ATP—GESGAGKT of the P-loop (132-139), NNNSSRFGK of switch I (190-198), and D414 of switch II [Fisher et al., 1995]. Other residues proposed to be involved in phosphate coordination, N76 and E221, are also well conserved across all MYO19 orthologs examined [Fisher et al., 1995]. Class XIX myosins contain a class-specific amino acid difference following the P-loop (Figure 1B). In 44 out of 45 MYO19 orthologs analyzed the residue following the P-loop is W, with *Daphnia* being the only exception (a cysteine). In the majority the approximately 2000 myosin sequences available in the alignments by Cope et al. [Cope et al. 1996] and Odrontiz et al. [Odronitz and Kollmar, 2007], the most common residue following the P-loop is either V or E. The much bulkier W is only found in class XIX orthologs within the set of sequences available at the time. This class-specific amino acid change immediately following the P-loop to a larger side chain might play a role in the affinity for nucleotide in the binding pocket, as threaded models of MYO19 suggest that W140 is positioned very close to the nucleotide binding site. It is also interesting to note that in kinesins this position is most often a Y, H, or F [Greene, et al., 2005] (The kinesin homepage, 2005), which also contain large side chains. The loop connecting the 25kD and 50kD subdomains of myosin, Loop 1, is part of a helix-loop-helix that spans the distance between the P-loop and switch I, straddling the nucleotide pocket [reviewed in Holmes, 2008]. Loop 1 varies in length between myosins, and this region of MYO19 is well conserved in both sequence and length among vertebrate orthologs. It is slightly shorter in length than longer Loop 1 regions such as those from MYH2 and MYO10, and longer in length than Loop 1 of MYO1C, MYO5A, and MYO6 (Figure 1B). Loop 1 appears to be involved in ADP release [Kurzawa-Goertz et al. 1998; Murphy and Spudich, 1998]. Switch I and Switch II are regions responsible for communicating nucleotide state to other regions of the molecule through interactions with the γ-phosphate of ATP [Smith and Rayment, 1996]. The sequence leading up to and including switch I

(179-198) is well conserved within MYO19 with some variability at position 191 (NxN) between species. In other myosins, the amino acid 4 residues prior to the NxN sequence is most often K. However, this is not the case in MYO19. In 39/45 orthologs this residue (186) is a cysteine, an amino acid difference found also in class IIIA and IIIB myosins as well as some insect class IC myosins. Switch II is extremely well conserved within class XIX myosins and varies little between myosin classes.

The converter region of myosins translates small conformational changes accompanying hydrolysis product release to large-scale movements of the long α-helix that makes up the lever arm. Although there is significant sequence variability within the converter region, there is not a great deal of diversity in length of converter regions, with a few notable exceptions. In most myosin sequences in the Cope alignment [Cope et al., 1996], the distance from strand 3 in β–sheet B (RCIxPN) to the conserved lysine in strand 3 in β–sheet F (T**K**xF) is approximately 60 amino acids. Additionally, the distance from the conserved lysine in beta sheet F to the beginning of the first IQ motif in the lever arm is 26 residues. Class VI myosins contain an insertion of approximately 38 amino acids between beta sheet F and the lever arm that reorients the lever arm relative to the core motor domain, resulting in a motor directed towards the actin minus-end [Menetrey et al., 2005]. Multiple sequence alignment of MYO19 with other myosins revealed a 30-35 amino acid insertion within the converter domain. Unlike MYO6, this insertion is not between the converter and the lever arm, and does not align with the MYO6 “reverse gear” (Figure 1C), suggesting that this sequence may serve a different function than the MYO6 “reverse gear.” It is interesting to note that the MYO19 insertion in the converter domain cannot be modeled onto existing myosin structures. The insertion is well-conserved within class XIX myosins, and comparison to the alignment by Odronitz and Kollmar. [Odronitz and Kollmar, 2007] reveals that other non-vertebrate classes (24B, 25, 26, 27) also contain insertions of greater than 10 amino acids within the converter domain.

The actin binding region of myosin consists of a number of loops and subdomains situated on both sides of a cleft, which is thought to close to facilitate strong binding of actin [reviewed in Holmes, 2008]. The binding of myosin to actin is partially dependent on electrostatic interactions between the two molecules. There are well-conserved regions in the actin binding domain of class XIX orthologs, particularly charged residues (Table I). Our analyses indicate that there are significant differences in the overall charge of the actin-interacting regions of MYO19 as compared to other myosins (Figure 2). Specifically, the Loop 2 region of MYO19 carries no net charge while it is positively charged in the other sequences to which it was compared. Loop 4 is more negatively charged than comparable regions in other myosins, while the HCM loop and the helix-turn-helix are more positively charged than in other myosins (Figure 2). Many of these regions are poorly resolved in available crystal structures of myosin, but have been modeled through a combination of cryo-electron microscopy, molecular dynamics, and other structural methods [Holmes et al., 2004; Lorenz and Holmes, 2010]. Threading of the human MYO19 sequence onto the modeled structure from Lorenz and Holmes [Lorenz and Holmes, 2010] reveals some conservation and some differences in the residues implicated in electrostatic interactions and hydrogen bonds between MYO19 and MYH2 (Figure 2). The positions of the changed resides in the MYO19 actin-binding region could play a role in the affinity of MYO19 for actin as well as in the ATPase activity. It has been reported that phosphorylation and mutations of residues in the actin binding loops alter the ATPase cycle kinetics. Heavy chain phosphorylation of some class I myosins occurs at the TEDS site in the hypertrophic cardiomyopathy loop [Bement and Mooseker, 1995]. Phosphorylation of MYO1C lead to increased ATPase activity by >20 fold but did not significantly affect the affinity of myosin for actin [Ostap et al., 2002]. Mutagenesis of a single charged residue in Loop 4 of smooth muscle myosin altered actomyosin affinity and doubled myosin *in vitro* motility velocity

[Ajtai et al., 2004]. In these instances, changes to the actin binding region that altered net charge impacted the mechanochemistry of the motor. Thus, the unique structural elements and amino acid charge composition in the actin binding region of MYO19 could play a critical role in defining its enzymatic and biochemical properties.

Expressed and purified MYO19 binds calmodulin via its IQ motifs

We coexpressed two versions of N-terminal FLAG-tagged human MYO19 with calmodulin in the baculovirus insect cell Sf9 system. MYO19-1IQ contains the motor domain and one IQ motif. MYO19-3IQ contains the motor domain followed by the lever arm consisting of three IQ motifs, the amino acid sequence used to generate an α-MYO19 antibody [Quintero et al., 2009], and a C-terminal 6x-His tag. Yields were approximately 0.15-0.5mg/L of Sf9 cells. The purity of MYO19 following FLAG affinity chromatography was ~90-95% as determined by Coomassie staining of SDS-PAGE gels (Figure 3). Both the MYO19-1IQ and MYO19-3IQ constructs bound and co-purified with calmodulin at the expected stoichiometries of 1.1±0.1 CaM/MYO19-1IQ (n=3 preparations) and 3.3±0.4 CaM/MYO19-3IQ (n=3 preparations). Furthermore, we obtained similar values by determining the amount of calmodulin bound to MYO19-3IQ after actin co-sedimentation (4.1±1.1 CaM/MYO19-3IQ ratio), and comparing the bound calmodulin to a standard curve of calmodulin in Coomassie stained SDS-PAGE gels. Experiments using purified MYO19 constructs *in vitro* were performed in KMg50DTT (50mM KCl, 10mM imidazole, 1mM EGTA, 1mM $MgCl_2$, 1mM DTT, pH 7.0) in the presence of 10μM calmodulin to ensure full occupancy of the IQ motifs. It has yet to be determined if proteins other than CaM serve as endogenous light chains of MYO19.

MYO19 encodes for an actin-activated ATPase

A hallmark of myosin motors is an actin-activated ATPase activity, and we chose to characterize this activity for MYO19 using the NADH-coupled assay [De La Cruz and Ostap, 2009; De La Cruz et al., 2000]. We measured the ATPase activity as a function of increasing concentrations of phalloidin-stabilized actin, in the presence of 1mM ATP and an ATP-regenerating system. With no actin present, the rate of ATPase activity for MYO19-1IQ (ν_0) was determined to be 0.03±0.01 s^{-1} (n=4 preparations). The maximal rate of actin-activated ATPase activity (k_{cat}) was calculated to be 2.2±0.2 s^{-1}, and the actin concentration at which ATPase activity was one-half of the maximal activity (K_{ATPase}) was found to be 20.1±3.7 μM (Figure 4A). Very similar results were observed for the MYO19-3IQ; ν_0 was found to be 0.03±0.01s^{-1} (n=3 preparations), k_{cat} found to be 2.7±0.2 s^{-1}, and K_{ATPase} found to be 26.5±5.4μM (Figure 4B). The intrinsic ATPase rate of MYO19-1IQ was verified through experiments with N-methylanthraniloyl-2′-deoxy-ATP (MANT-dATP). The fluorescence of MANT-dATP is enhanced upon binding to the active site of myosins, and decreases upon MANT-dADP dissociation. By mixing 0.25μM MANT-dATP at with 0.5μM MYO19-1IQ and fitting the observed fluorescence decrease to a single exponential decay, the intrinsic ATPase activity of MYO19-1IQ was estimated to be 0.03±0.01 s^{-1}, which is in agreement with the value as measured by the NADH-coupled assay (Figure 4C).

MYO19 steady-state kinetics show an actin-activated ATPase activity that is neither the slowest nor the fastest among the myosin family, and low to medium concentrations of actin are required to fully activate the ATPase. Other characterized motors with similar rates of actin activated ATPase include human MYO1C [El Mezgueldi et al. 2002], chicken smooth muscle myosin [Cremo and Geeves, 1998; Marston and Taylor, 1980; Rosenfeld et al., 2000], MYO3A [Dose et al., 2007], *Drosophila* MYO7A [Yang et al. 2006], mouse MYO7B [Henn and De La Cruz, 2005] and bovine MYO10 [Kovacs et al., 2005]. However, some of these myosins differ from MYO19 when comparing the K_{ATPase} value. For human

MYO1C, *Drosophila* MYO7A, and mouse MYO7B, the K_{ATPase} is an order of magnitude lower than that of MYO19.

MYO19 populates high actin affinity states in the presence of ATP

Determination of the fraction of MYO19 bound to actin is an indication of the fraction of MYO19 that is populating actin-bound states under steady-state conditions. We performed MYO19 cosedimentation assays with increasing concentrations of phalloidin-stabilized actin in the presence of 2mM ATP and an ATP regenerating system. We then measured the fraction of MYO19-1IQ that was associated with the actin pellet (Figure 4D). The maximum fraction bound was measured to be 0.77±0.03 (n=3 preparations). These data were fit to a hyperbola to determine the steady-state actin affinity, K_{actin} =1.2±0.2μM. A rigor-bound control sample was run as well (5μM actin, no ATP, no regenerating system), and the fraction of actin-bound MYO19-1IQ found to be 0.80±0.01. To account for the possibility of ADP accumulation during the assay, we repeated the experiments eliminating the 10-minute room temperature incubation in the presence of ATP, and measured ADP levels in the supernatant at the end of the experiment using the NADH-linked assay. When the 10-minute prespin incubation with ATP was not included in the assay, the values were similar (maximum fraction bound = 0.94±0.05 and K_{actin} = 3.0±0.6μM). ADP levels were approximately 0.2mM in the supernatants at the end of the assay, which is less than 10% of the initial ATP concentration.

Cosedimentation assays reveal that MYO19 populates high actin affinity states in the presence of ATP, suggesting that it has an intermediate to high duty ratio. Alternatively, MYO19 may contain a high affinity for actin in the “traditional” weakly bound states. Other myosins that also populate high affinity states in the presence of ATP include MYO5 [De La Cruz et al., 1999; Yengo et al. 2002] and MYO3A [Dose et al., 2007]. The observed affinity of MYO19 for actin in the steady-state may be due to the amino acid differences in the putative actin-binding interface revealed by our sequence analysis. Alternatively, MYO19 may have a high affinity for ADP, which results in the actomyosin·ADP state predominantly being populated in the cosedimentation assay. Nevertheless, the results suggest that under near physiological conditions MYO19 contains a relatively high steady-state affinity for actin.

Interestingly, MYO19 contains a K_{Actin} that is 10-fold lower than the K_{ATPase} measured in the steady-state ATPase assays. This property was also observed in MYO9B [Nalavadi et al., 2005], which is a monomeric myosin that contains a large insert in the actin binding region. When this large insert in Loop 2 was removed from MYO9B, its actin affinity was significantly reduced. Loop 2 is known to contribute to actin affinity in the weak binding states through charge interactions [Joel et al., 2003; Yengo and Sweeney, 2004]. MYO19 also contains a divergent Loop 2 sequence. Rather than containing a large insertion, Loop 2 of MYO19 lacks positive charge. Therefore, the highly positively charged HCM loop and helix-turn-helix may play roles in enhancing the steady-state actin affinity of MYO19, as compared to other myosins.

MYO19-3IQ catalyzes translocation of actin filaments, in vitro

The velocity of MYO19-mediated movements were measured *in vitro* using the actin gliding filament assay in the presence of an ATP regeneration system, at a range of ATP concentrations [Kron et al., 1992]. MYO19-3IQ protein was adhered to nitrocellulose-coated slides via antibody interactions with either the antibody target site following the third IQ motif, or the C-terminal 6×His tag. ATP-dependent movements of fluorescently-labeled actin filaments were observed in all cases (Figure 5A). Velocities ranged from 144±3 nm/s at 0.1mM ATP to 229±4 nm/s at 2mM ATP. Fitting the data to the equation of a hyberbola

and assuming velocity in the absence of ATP was zero resulted in a V_{max} of approximately 220 nm/s, a value similar to what was measured at 2mM ATP (Figure 5B).

Previously observed gain-of-function is dependent on motor activity

Ectopic expression of GFP-tagged, full length MYO19 in cultured A549 pulmonary epithelial cells resulted in a gain-of-function where the entire mitochondrial network displayed increased dynamics as measured by displacement index (DI) [Caviston et al., 2011; Quintero et al., 2009]. With a DI of approximately 1, the mitochondrial network in A549 cells under control conditions is not highly dynamic across the timescales observed in this experiment [Quintero et al., 2009] (Supplemental Figure 4). We hypothesized that the functional gain was mediated by MYO19 motor activity via its ATPase, and chose to test the hypothesis using the same DI assay with a GFP-tagged MYO19 with impaired motor activity. Mutation of G135 to R is hypothesized to disrupt ATP binding and result in a rigor-like mutant [Bejsovec and Anderson, 1990; Lechler et al., 2000]. Similar to what had been previously observed, ectopic expression of wild type, full length GFP-MYO19 resulted in an increased DI when compared to cells expressing GFP-MYO19 tail, a construct lacking the motor domain entirely. Expressed GFP-MYO19-G135R localized to mitochondria, but did not result in the gain-of-function observed with the wild type protein, indicating a requirement for a functional motor domain in the gain-of-function phenotype (Figure 5C). Introduction of the G135R mutation into MYO19-1IQ resulted in a 1.5-fold reduction in endogenous ATPase activity and a 3.3-fold reduction in actin-activated ATPase activity at 30μM F-actin ($0.3\pm0.1\ s^{-1}$), when compared to wild-type MYO19-1IQ ($1.3\pm0.3\ s^{-1}$), *in vitro* (Supplemental Figure 5). Although not a complete elimination of ATPase activity, the observations are consistent with a reduction in motor activity disrupting MYO19-induced dynamics.

MYO19 in the context of the cell

Here we demonstrate that the motor domain of human MYO19 contains biochemical properties predicted for a myosin. Human MYO19 constructs contain an actin-activated ATPase with the ability to: bind actin in an ATP-dependent manner, bind a common myosin light chain, and translocate actin filaments *in vitro*. Inactivating mutations result in diminished ATPase activity and do not induce the gain-of-function observed with the wild-type protein. Based on our analyses, class XIX myosins show sequence similarity to other myosins that allow for comparison between myosin genes by both sequence alignment and threading to crystal structures of well-characterized myosins. Comparisons based on these similarities allowed for the identification of regions of “conserved difference” within class XIX myosin orthologs that suggested differences in chemomechanical properties of MYO19. These differences in key sequences essential for myosin function (such as the nucleotide binding region, actin binding region, and lever arm) are not found in other myosin classes. The chemomechanical properties of MYO19 are important determinants of the class-specific functional differences related to the cellular roles of MYO19.

These data suggest that MYO19 could serve as a mitochondrial anchor under the proper cellular conditions. It has been shown that growth factor-induced docking of mitochondria may involve actin, as pharmacologic depletion of F-actin reduces accumulation of mitochondria at sites of induced growth factor signaling [Chada and Hollenbeck, 2004]. In *Drosophila* neuronal cells myosin V and VI have been reported to oppose long range MT based movements and facilitate docking of the organelle [Pathak et al., 2010]. The kinetics of the motor also support the possibility that a docking mechanism could ensure that mitochondria stay bound in areas where the regional concentration of ADP is high or ATP is low. The cosedimentation data indicate that under steady-state conditions, MYO19 contains a high steady-state affinity for actin. In our assays, most of the MYO19 was actin-bound

(cosedimentation assay) at actin concentrations that were sub-saturating in the steady-state ATPase assay. The fact that $K_{actin} < K_{ATPase}$, suggests that the rate-limiting step occurs when MYO19 is actin-bound [Howard, 2001]. For many high-duty ratio myosins, the release of ADP from the nucleotide binding site of actin-bound myosin is the rate-limiting step [De La Cruz and Ostap, 2004]. Therefore, under conditions where local ADP concentrations were elevated, such a motor would likely remain actin-bound. As MYO19 is linked to one of the major sources of cellular ATP (the mitochondrion), it is possible that MYO19 may be serving as an inherent ATP sensor, anchoring the mitochondrion to actin where local ADP concentrations are high, and moving mitochondria away from high local ATP concentrations through motility (Figure 6).

Although evidence does not yet exist to indicate whether MYO19 functions as a monomer, it could work in high densities to create an effective duty-ratio capable of producing directed cargo transport. Myosin-I and most characterized myosin-II isoforms must work in ensembles of many motors to generate movement along an actin filament as *in vitro* studies show that sliding is a function of protein density [Finer et al., 1994; Harada et al., 1990; Uyeda et al., 1990]. Thus, MYO19 might utilize this mechanism to "motor" when the concentration of MYO19 on the mitochondria reaches a level capable of inducing movement. However, MYO19 at high densities on the mitochondrial outer membrane could interfere with motility. Previously we observed that ectopic expression of MYO19 leads to a decreased velocity of mitochondria and a morphological change in which mitochondria have a tadpole-like shape where the leading edge is wider than the trailing edge [Quintero et al., 2009]. By increasing the motor density past some threshold level, it is possible that some MYO19-actin interactions were inducing a drag-like force on the organelle, both slowing the movements and altering the geometry of the organelle. Such an effect would be more dramatic for a motor which spends a large fraction of its chemomechanical cycle in the actin-bound states.

Taken together these data lead us to a model in which the local ratio of [ADP] to [ATP] is among the factors that might regulate the function of MYO19, resulting in a system in which the mitochondria can be effectively positioned in regions of the cell where they are most needed. We cannot fail to recognize that there are also other motors present on mitochondria that could impact the dynamic distribution of this organelle. Mechanisms coordinating the activities of multiple motor species exist for other organelle systems and such regulatory mechanisms remain to be characterized for mitochondria motors.

Materials and Methods

Sequence Analysis

We performed a sequence comparison to determine the sequence variability in the conserved regions of the MYO19 motor with respect to the conserved regions of other myosins. The core motor domain of Human MYO19 (corresponding to amino acids 37-750 of human MYO19 [Quintero et al., 2009], NP_001157207, was directly aligned against the core motor domain of five other myosins using ClustalX 2.1 (multiple alignment mode, default settings) [Larkin et al. 2007]: rabbit MYH2 (skeletal) XP_002718996.1, chicken MYO5A NP_990631.1, pig MYO6 NP_999186.1, cow MYO10 NP_776819.1, and human MYO1C NP_001074248.1. These species were selected for alignment due to the availability of biochemical data (reviewed in [El-Mezgueldi and Bagshaw, 2008]). Regions of the aligned sequences were then selected for comparison based on the previously described variably conserved regions [Cope et al., 1996], including conserved regions in the ATP binding domain (P-loop, Loop 1, Switch I, Switch II) and the actin binding region (Loop-2, Loop-3, Loop-4, HMC loop, the helix-loop-helix). These regions were evaluated based on length, sequence, and net charge. To determine if the sequence changes observed in human MYO19

as compared to the other 5 myosins were unique to MYO19, the sequences were compared to the alignment of 143 myosin sequences by Cope et al. [Cope et al. 1996] and of 1984 sequences by Odronitz and Kollmar [Odronitz and Kollmar, 2007].

We identified the class-XIX specific amino acid differences by aligning the human MYO19 core motor domains with 41 other MYO19 orthologs obtained from the NCBI database, the Ensembl Genome Browser, and supplementary data from Odronitz and Kollmar [Odronitz and Kollmar, 2007] using ClustalX 2.1 multiple alignment mode with default settings. Included sequences consisted of a combination of verified and predicted gene products. Three of the identified MYO19 orthologs were excluded based on the incomplete nature of the sequence (Supplemental Table I). A phylogenetic tree of all 45 sequences was generated using the neighbor joining and bootstrap method (1000 replicates) in ClustalX2.1, and drawn using FigTree v 1.3.1.

Computer modeling/threading

To determine a likely tertiary structure for MYO19, amino acids 1-827 of the human MYO19 sequence were submitted to the Protein Homology/analogy Recognition Engine (Phyre2) web server. Briefly, the engine uses homology identification and secondary structure prediction to determine structural homologues by a profile-profile alignment algorithm [Kelley and Sternberg, 2009]. High scoring alignments are then used to construct a three-dimensional model of the submitted sequence.

Since the regions of myosins directly involved in the actin binding interface are not well resolved in the structures generated via X-ray crystallography, but have been positioned through a combination of modeling crystallography and cryo-electron microscopy [Holmes and Geeves 2000; Holmes et al., 2004; Rayment et al., 1993], Phyre2 was also used to predict the structure of the actin-binding interface of MYO19 by aligning the human MYO19 sequence directly to the actomyosin structure by Lorenz and Holmes [Lorenz and Holmes, 2010].

Expression Plasmids

Five expression plasmids were generated via PCR cloning, restriction digestion, and ligation into expression plasmids, using the human MYO19 coding sequence as the template. A construct consisting of an N-terminal FLAG tag and amino acids 2-848 consisting of the motor domain and 3 IQ motifs, and a C-terminal 6×His tag (MYO19-3IQ) was generated in the pFastbac plasmid by adding the restriction site for EcoRI at the 5′-end and the coding sequence for 6×His and a restriction site for SalI at the 3′ end via PCR, and then inserting the product into the vector via restriction digestion and ligation. The FLAG-tag was then added at the N-terminus via PCR mutagenesis, removing the EcoRI restriction site in the process. To generate a construct consisting of an N-terminal FLAG-tag, the motor domain, and one IQ motif (amino acids 2-787), a stop codon was inserted following the codon for amino acid 787 via PCR mutagenesis. peGFP-MYO19 and peGFP-MYO19 tail were generated as previously described [Quintero et al., 2009]. peGFP-MYO19-G135R contains an inactivating point-mutation in the motor domain thought to generate a motor with impaired nucleotide binding ability [Bejsovec and Anderson, 1990; Lechler et al., 2000] and was generated by PCR mutagenesis. A table of primers used in this study can be found in Supplemental Table II.

Protein Purification

A construct of MYO19 1IQ and 3IQ was generated by inserting the above mentioned cDNA clones into pFastbac (Invitrogen). Recombinant baculovirus were generated using standard protocols and MYO19 proteins were purified from Sf9 cells as previously described [Dose

et al. 2007; Dose et al. 2008]. Suspension cultures of Sf9 cells were infected with baculovirus containing sequences encoding for expression of calmodulin and baculovirus containing sequences encoding for expression of a MYO19 construct. Cells were allowed to grow for 3-days at 28°C with shaking, and were then pelleted at 5000×g for 30 minutes. Cell pellets were resuspended in lysis buffer (10mM Tris-HCl, 400mM KCl, 1mM EDTA, 1mM EGTA, 2mM $MgCl_2$, 2mM ATP, 2mM DTT, 0.01mg/ml aprotinin, 0.1mg/ml leupeptin, 1mM PMSF, 0.5% Igepal, 5% sucrose, pH 7.5) and lysed by homogenization in a Dounce homogenizer with a Teflon pestle. Lysates were cleared by centrifugation at 180,000×g for 1 hour (4°C). Supernatants were run over FLAG affinity resin, washed in wash buffer (10mM Tris-HCl, 200mM KCl, 1mM EDTA, 1mM EGTA, 2mM $MgCl_2$, 2mM ATP, 2mM DTT, 0.01mg/ml aprotinin, 0.1mg/ml leupeptin, 1mM PMSF, 5μg/ml calmodulin, pH 7.5), and then eluted by gravity flow in a small volume of wash buffer containing FLAG peptide [Wang et al. 1998]. The elute was concentrated using at centricon spin concentrator, and then dialyzed against KMg50DTT (50mM KCl, 10mM imidazole, 1mM EGTA, 1mM $MgCl_2$, 1mM DTT, pH 7.0). Calmodulin was expressed and purified in bacteria as described [Putkey et al., 1985]. Actin was purified from acetone powder generated from rabbit skeletal muscle myosin [Pardee and Spudich, 1982], and all experiments contained equimolar phalloidin.

Steady State ATPase Assay

MYO19 ATPase activity in the presence of increasing actin concentration was determined via the NADH-linked assay, as previously described [De La Cruz and Ostap, 2009; De La Cruz et al., 2000]. The reaction mixture contained 0.1μM MYO19 protein in reaction buffer (KMg50DTT, pH 7.0 supplemented with 0.2mM NADH, 10U/mL lactate dehydrogenase, 0.5U/mL phosphoenol pyruvate, 45U/mL pyruvate kinase). To determine actin activation, reaction mixtures containing increasing concentrations of actin were mixed and placed on ice. Prior to the start of the assay, 1mM ATP was added to the reaction mixture. The absorbance at 340nm was observed for 2 minutes (25°C) using an Applied Photophysics SX. 18MV-R stopped-flow reaction analyzer. Absorbance traces were fit to the equation of a line, and velocities ($ATP{\cdot}s^{-1}$) were determined from the calculated slope, MYO19 concentration, and extinction coefficient of NADH. Rates were corrected for the ATPase activity of F-actin by subtracting the calculated velocity for the appropriate actin-only control from the actoMYO19 samples. The turnover number (k_{cat}) and Michaelis-Menten constant with respect to [actin] (K_{ATPase}) were calculated by fitting the plot of reaction velocity versus [Actin] to the equation of a hyberbola.

Cosedimentation Assay

To determine the fraction of MYO19 associated with actin under steady-state conditions, actin cosedimentation assays were performed [De La Cruz and Ostap, 2009]. Increasing concentrations of actin were incubated with 0.5μM MYO19 in KMg50DTT reaction buffer without lactate dehydrogenase supplemented to 2mM $MgCl_2$ and allowed to incubate on ice for 10 minutes, then allowed to equilibrate to room temperature for 10 minutes. The tubes were incubated at room temperature for 10 minutes following the addition of ATP to a final concentration of 2mM. Samples were then centrifuged at 320,000×g for 15 minutes (25°C). The supernatants were removed, and pellets resuspended in 8M urea. Pellet and supernatant samples were separated by SDS-PAGE, stained with Coomassie blue, and the fraction of MYO19 in the supernatant and pellet was calculated by densitometry analysis using ImageJ [Abramoff et al., 2004]. For each experiment a “rigor” control at 5μM actin with no ATP added was also run in parallel.

Calculation of CaM/MYO19 ratio

The relative amount of calmodulin bound to MYO19 was calculated via densitometry of samples from cosedimentation assays. The samples were prepared as described above, and the density of the MYO19 and calmodulin bands were determined. To calculate the ratio of CaM per MYO19, the measured density of the bands were divided by their molecular weights to determine relative molar amounts, and then the relative molar amount of CaM was divided by the relative molar amount of MYO19. The intensity of the calmodulin band associated with the actin-bound MYO19-3IQ/CaM complex after actin co-sedimentation was compared to a standard curve of calmodulin on the same SDS-PAGE gel to determine the stoichiometry of the MYO19-3IQ/CaM complex.

In vitro motility Assay

The velocity of MYO193IQ-mediated actin movements was determined via the *in vitro* actin gliding assay as described previously [Kron et al., 1992]. In a flow cell assembled from a nitrocellulose-coated coverslip (22×22mm, #1.5), glass slide, and double-sided tape. The flow cell was incubated with 0.12μg/ml anti-MYO19 antibody [Quintero et al., 2009] in KMg50 for two minutes, washed twice with 1mg/ml bovine serum albumin in KMg50, and then rinsed with KMg50. 0.25μM MYO19-3IQ in KMg50 was allowed to bind in the flow cell for 2 minutes, and then washed with KMg50. 10nM Rhodamine-labeled f-actin was added, followed by the addition of KMg50DTT activation buffer (KMg50DTT, pH7.0, 0.7% methyl cellulose, 5μM CaM, 1mg/mL BSA, 3 mg/ml glucose, 2.5 mM phosphoenol pyruvate, 20 units/ml pyruvate kinase, 0.1 mg/ml glucose oxidase, and 0.018 mg.ml catalase). The flow cell was imaged via time-lapse microscopy using a Nikon TE2000-PFS equipped with a 60×/1.4NA lens and a Coolsnap HQ2 cooled CCD camera controlled using Nikon Elements 3.0. Velocity was calculated using the ImageJ plugin in, MtrackJ [Meijering et al., 2012] as the change in distance divided by elapsed time.

Mammalian Cell Culture and transfection

Human pulmonary carcinoma cells, A549 [Lieber et al., 1976], were maintained in culture in F12K medium supplemented with 10% fetal bovine serum, penicillin (50U/ml), and streptomycin(50μg/ml), at 37°C in an atmosphere of 5% CO_2, as described previously [Quintero et al. 2009]. For expression of GFP-tagged constructs, cells were transfected using Fugene HD transfection reagent according to the manufacturer's protocol. Briefly, 30,000 cells were plated into wells of a 6-well plate containing a 22×22mm #1.5 coverslip and allowed to adhere overnight. Plasmid DNA/Fugene HD complexes were then added to each well (1μg-2μg DNA per well) and allowed to incubate with the cells for 18-30 hours before imaging.

Displacement Index Assay

Ectopic expression of full length GFP-MYO19 has been shown to lead to a gain-of-function where the dynamics of the mitochondrial network are increased [Quintero et al. 2009]. The displacement index for GFP-MYO19-G135R was measured and compared to that for GFP-MYO19 tail and GFP-MYO19. Briefly, A549 cells expressing a GFP-MYO19 construct were placed in a Rose chamber filled with OptiMem without phenol red containing Penicillin and streptomycin and maintained at ∼32°C on the microscope stage. The cells were imaged via time-lapse microscopy using a Nikon TE2000-PFS equipped with a 60×/1.4NA lens and a Coolsnap HQ2 cooled CCD camera controlled using Nikon Elements 3.0. Cells were imaged for 40 frames with a 5-second interval between frames. Metamorph 5.07 was used to calculate displacement index by applying a threshold to the image stacks that defined the area containing mitochondria. The stack was maximum projected to determine the total area which contained mitochondria at any point during the image acquisition.

Displacement index was calculated by dividing the area calculated from the maximum projection by the area containing mitochondria in the first frame. If the network was not dynamic, then the DI would be close to 1. If the mitochondrial network displayed dynamics over the course of the movie, then DI would be a value greater than 1.

Supplementary Material

Refer to Web version on PubMed Central for supplementary material.

Acknowledgments

RCA was supported in this work by the Feldman-Koster and Ellen P. Reese Funds for undergraduate independent research from Mount Holyoke College. CMY was supported by NIH EY018141 and a grant from the Pennsylvania Department of Health (4100050904). OAQ was supported by a grant from the National Cancer Institute at the NIH (K01CA160667). We would like to thank Kenneth Holmes for providing the coordinate file for the actin-bound MYH2 model, Elizabeth Schinski for assistance with experiments in response to reviewer's comments, and Sarah Friday for illustrating Figure 6. We would also like to thank Darshan Trivedi, Lorna Silipino, Anja Swenson, Lindsay Case, Sadie Ingle, and Uri Manor for assistance and discussion.

References

Abramoff MD, Magalhaes PJ, Ram SJ. Image Processing with ImageJ. Biophotonics International. 2004; 11(7):36–42.

Ajtai K, Garamszegi SP, Watanabe S, Ikebe M, Burghardt TP. The myosin cardiac loop participates functionally in the actomyosin interaction. J Biol Chem. 2004; 279(22):23415–21. [PubMed: 15020589]

Altmann K, Frank M, Neumann D, Jakobs S, Westermann B. The class V myosin motor protein, Myo2, plays a major role in mitochondrial motility in Saccharomyces cerevisiae. J Cell Biol. 2008; 181(1):119–30. [PubMed: 18391073]

Bejsovec A, Anderson P. Functions of the myosin ATP and actin binding sites are required for C. elegans thick filament assembly. Cell. 1990; 60(1):133–40. [PubMed: 2136805]

Bement WM, Mooseker MS. TEDS rule: a molecular rationale for differential regulation of myosins by phosphorylation of the heavy chain head. Cell Motil Cytoskeleton. 1995; 31(2):87–92. [PubMed: 7553910]

Boldogh IR, Pon LA. Interactions of mitochondria with the actin cytoskeleton. Biochim Biophys Acta. 2006; 1763(5-6):450–62. [PubMed: 16624426]

Boldogh IR, Yang HC, Nowakowski WD, Karmon SL, Hays LG, Yates JR 3rd, Pon LA. Arp2/3 complex and actin dynamics are required for actin-based mitochondrial motility in yeast. Proc Natl Acad Sci U S A. 2001; 98(6):3162–7. [PubMed: 11248049]

Caviston JP, Zajac AL, Tokito M, Holzbaur EL. Huntingtin coordinates the dynein-mediated dynamic positioning of endosomes and lysosomes. Mol Biol Cell. 2011; 22(4):478–92. [PubMed: 21169558]

Chada SR, Hollenbeck PJ. Nerve growth factor signaling regulates motility and docking of axonal mitochondria. Curr Biol. 2004; 14(14):1272–6. [PubMed: 15268858]

Combet C, Jambon M, Deleage G, Geourjon C. Geno3D: automatic comparative molecular modelling of protein. Bioinformatics. 2002; 18(1):213–4. [PubMed: 11836238]

Cope MJ, Whisstock J, Rayment I, Kendrick-Jones J. Conservation within the myosin motor domain: implications for structure and function. Structure. 1996; 4(8):969–87. [PubMed: 8805581]

Coureux PD, Sweeney HL, Houdusse A. Three myosin V structures delineate essential features of chemo-mechanical transduction. EMBO J. 2004; 23(23):4527–37. [PubMed: 15510214]

Cremo CR, Geeves MA. Interaction of actin and ADP with the head domain of smooth muscle myosin: implications for strain-dependent ADP release in smooth muscle. Biochemistry. 1998; 37(7):1969–78. [PubMed: 9485324]

De La Cruz EM, Ostap EM. Relating biochemistry and function in the myosin superfamily. Curr Opin Cell Biol. 2004; 16(1):61–7. [PubMed: 15037306]

De La Cruz EM, Ostap EM. Kinetic and equilibrium analysis of the myosin ATPase. Methods Enzymol. 2009; 455:157–92. [PubMed: 19289206]

De La Cruz EM, Sweeney HL, Ostap EM. ADP inhibition of myosin V ATPase activity. Biophys J. 2000; 79(3):1524–9. [PubMed: 10969013]

De La Cruz EM, Wells AL, Rosenfeld SS, Ostap EM, Sweeney HL. The kinetic mechanism of myosin V. Proc Natl Acad Sci U S A. 1999; 96(24):13726–31. [PubMed: 10570140]

De Vos KJ, Allan VJ, Grierson AJ, Sheetz MP. Mitochondrial function and actin regulate dynamin-related protein 1-dependent mitochondrial fission. Curr Biol. 2005; 15(7):678–83. [PubMed: 15823542]

Dekker-Ohno K, Hayasaka S, Takagishi Y, Oda S, Wakasugi N, Mikoshiba K, Inouye M, Yamamura H. Endoplasmic reticulum is missing in dendritic spines of Purkinje cells of the ataxic mutant rat. Brain Res. 1996; 714(1-2):226–30. [PubMed: 8861629]

Dose AC, Ananthanarayanan S, Moore JE, Burnside B, Yengo CM. Kinetic mechanism of human myosin IIIA. J Biol Chem. 2007; 282(1):216–31. [PubMed: 17074769]

Dose AC, Ananthanarayanan S, Moore JE, Corsa AC, Burnside B, Yengo CM. The kinase domain alters the kinetic properties of the myosin IIIA motor. Biochemistry. 2008; 47(8):2485–96. [PubMed: 18229949]

DuBoff B, Gotz J, Feany MB. Tau promotes neurodegeneration via DRP1 mislocalization in vivo. Neuron. 2012; 75(4):618–32. [PubMed: 22920254]

El-Mezgueldi, M.; Bagshaw, CR. The Myosin Family: Biochemical and Kinetic Properties. In: Coluccio, LM., editor. Myosins: A Superfamily of Molecular Motors. Dordrecht: Springer; 2008. p. 55-93.

El Mezgueldi M, Tang N, Rosenfeld SS, Ostap EM. The kinetic mechanism of Myo1e (human myosin-IC). J Biol Chem. 2002; 277(24):21514–21. [PubMed: 11940582]

Finer JT, Simmons RM, Spudich JA. Single myosin molecule mechanics: piconewton forces and nanometre steps. Nature. 1994; 368(6467):113–9. [PubMed: 8139653]

Fisher AJ, Smith CA, Thoden JB, Smith R, Sutoh K, Holden HM, Rayment I. X-ray structures of the myosin motor domain of Dictyostelium discoideum complexed with MgADP.BeFx and MgADP.AlF4. Biochemistry. 1995; 34(28):8960–72. [PubMed: 7619795]

Flicek P, Amode MR, Barrell D, Beal K, Brent S, Carvalho-Silva D, Clapham P, Coates G, Fairley S, Fitzgerald S, et al. Ensembl 2012. Nucleic Acids Res. 2012; 40(Database issue):D84–90. [PubMed: 22086963]

Harada Y, Sakurada K, Aoki T, Thomas DD, Yanagida T. Mechanochemical coupling in actomyosin energy transduction studied by in vitro movement assay. J Mol Biol. 1990; 216(1):49–68. [PubMed: 2146398]

Henn A, De La Cruz EM. Vertebrate myosin VIIb is a high duty ratio motor adapted for generating and maintaining tension. J Biol Chem. 2005; 280(47):39665–76. [PubMed: 16186105]

Hollenbeck PJ, Saxton WM. The axonal transport of mitochondria. J Cell Sci. 2005; 118(Pt 23):5411–9. [PubMed: 16306220]

Holmes, KC. Myosin Structure. In: Collucio, LM., editor. Myosins. Springer; Netherlands: 2008. p. 35-54.

Holmes KC, Geeves MA. The structural basis of muscle contraction. Philos Trans R Soc Lond B Biol Sci. 2000; 355(1396):419–31. [PubMed: 10836495]

Holmes KC, Schroder RR, Sweeney HL, Houdusse A. The structure of the rigor complex and its implications for the power stroke. Philos Trans R Soc Lond B Biol Sci. 2004; 359(1452):1819–28. [PubMed: 15647158]

Howard, J. Mechanics of Motor Proteins and the Cytoskeleton. Sudnerland, MA: Sinauer Associates, Inc; 2001. p. 229-244.

Joel PB, Sweeney HL, Trybus KM. Addition of lysines to the 50/20 kDa junction of myosin strengthens weak binding to actin without affecting the maximum ATPase activity. Biochemistry. 2003; 42(30):9160–6. [PubMed: 12885250]

Kelley LA, Sternberg MJ. Protein structure prediction on the Web: a case study using the Phyre server. Nat Protoc. 2009; 4(3):363–71. [PubMed: 19247286]

Korobova F, Ramabhadran V, Higgs HN. An actin-dependent step in mitochondrial fission mediated by the ER-associated formin INF2. Science. 2013; 339(6118):464–7. [PubMed: 23349293]

Kovacs M, Wang F, Sellers JR. Mechanism of action of myosin X, a membrane-associated molecular motor. J Biol Chem. 2005; 280(15):15071–83. [PubMed: 15705568]

Kron SJ, Drubin DG, Botstein D, Spudich JA. Yeast actin filaments display ATP-dependent sliding movement over surfaces coated with rabbit muscle myosin. Proc Natl Acad Sci U S A. 1992; 89(10):4466–70. [PubMed: 1533933]

Kurzawa-Goertz SE, Perreault-Micale CL, Trybus KM, Szent-Gyorgyi AG, Geeves MA. Loop I can modulate ADP affinity, ATPase activity, and motility of different scallop myosins. Transient kinetic analysis of S1 isoforms. Biochemistry. 1998; 37(20):7517–25. [PubMed: 9585566]

Larkin MA, Blackshields G, Brown NP, Chenna R, McGettigan PA, McWilliam H, Valentin F, Wallace IM, Wilm A, Lopez R, et al. Clustal W and Clustal X version 2.0. Bioinformatics. 2007; 23(21):2947–8. [PubMed: 17846036]

Lechler T, Shevchenko A, Li R. Direct involvement of yeast type I myosins in Cdc42-dependent actin polymerization. J Cell Biol. 2000; 148(2):363–73. [PubMed: 10648569]

Lieber M, Smith B, Szakal A, Nelson-Rees W, Todaro G. A continuous tumor-cell line from a human lung carcinoma with properties of type II alveolar epithelial cells. Int J Cancer. 1976; 17(1):62–70. [PubMed: 175022]

Lisé MF, Wong TP, Trinh A, Hines RM, Liu L, Kang R, Hines DJ, Lu J, Goldenring JR, Wang YT, et al. Involvement of Myosin Vb in Glutamate Receptor Trafficking. Journal of Biological Chemistry. 2006; 281(6):3669–3678. [PubMed: 16338934]

Lorenz M, Holmes KC. The actin-myosin interface. Proc Natl Acad Sci U S A. 2010; 107(28):12529–34. [PubMed: 20616041]

Marston SB, Taylor EW. Comparison of the myosin and actomyosin ATPase mechanisms of the four types of vertebrate muscles. J Mol Biol. 1980; 139(4):573–600. [PubMed: 6447797]

McConnell RE, Tyska MJ. Leveraging the membrane - cytoskeleton interface with myosin-1. Trends Cell Biol. 2010; 20(7):418–26. [PubMed: 20471271]

Meijering E, Dzyubachyk O, Smal I. Methods for cell and particle tracking. Methods Enzymol. 2012; 504:183–200. [PubMed: 22264535]

Menetrey J, Bahloul A, Wells AL, Yengo CM, Morris CA, Sweeney HL, Houdusse A. The structure of the myosin VI motor reveals the mechanism of directionality reversal. Nature. 2005; 435(7043): 779–85. [PubMed: 15944696]

Minin AA, Kulik AV, Gyoeva FK, Li Y, Goshima G, Gelfand VI. Regulation of mitochondria distribution by RhoA and formins. J Cell Sci. 2006; 119(Pt 4):659–70. [PubMed: 16434478]

Miyata M, Finch EA, Khiroug L, Hashimoto K, Hayasaka S, Oda SI, Inouye M, Takagishi Y, Augustine GJ, Kano M. Local Calcium Release in Dendritic Spines Required for Long-Term Synaptic Depression. Neuron. 2000; 28(1):233–244. [PubMed: 11086997]

Mooseker, MS.; Foth, BJ. The Structural And Functional Diversity Of The Myosin Family Of Actin-Based Molecular Motors. In: Coluccio, LM., editor. Myosins. Springer; Netherlands: 2008. p. 1-34.

Morris RL, Hollenbeck PJ. Axonal transport of mitochondria along microtubules and F-actin in living vertebrate neurons. J Cell Biol. 1995; 131(5):1315–26. [PubMed: 8522592]

Murphy CT, Spudich JA. Dictyostelium myosin 25-50K loop substitutions specifically affect ADP release rates. Biochemistry. 1998; 37(19):6738–44. [PubMed: 9578557]

Nalavadi V, Nyitrai M, Bertolini C, Adamek N, Geeves MA, Bahler M. Kinetic mechanism of myosin IXB and the contributions of two class IX-specific regions. J Biol Chem. 2005; 280(47):38957–68. [PubMed: 16179355]

Odronitz F, Kollmar M. Drawing the tree of eukaryotic life based on the analysis of 2,269 manually annotated myosins from 328 species. Genome Biol. 2007; 8(9):R196. [PubMed: 17877792]

Ostap EM, Lin T, Rosenfeld SS, Tang N. Mechanism of regulation of Acanthamoeba myosin-IC by heavy-chain phosphorylation. Biochemistry. 2002; 41(41):12450–6. [PubMed: 12369835]

Pardee JD, Spudich JA. Purification of muscle actin. Methods Enzymol. 1982; 85 Pt B:164–81. [PubMed: 7121269]

Pathak D, Sepp KJ, Hollenbeck PJ. Evidence that myosin activity opposes microtubule-based axonal transport of mitochondria. J Neurosci. 2010; 30(26):8984–92. [PubMed: 20592219]

Putkey JA, Slaughter GR, Means AR. Bacterial expression and characterization of proteins derived from the chicken calmodulin cDNA and a calmodulin processed gene. J Biol Chem. 1985; 260(8): 4704–12. [PubMed: 2985564]

Quintero OA, DiVito MM, Adikes RC, Kortan MB, Case LB, Lier AJ, Panaretos NS, Slater SQ, Rengarajan M, Feliu M, et al. Human Myo19 is a novel myosin that associates with mitochondria. Curr Biol. 2009; 19(23):2008–13. [PubMed: 19932026]

Rayment I, Holden HM, Whittaker M, Yohn CB, Lorenz M, Holmes KC, Milligan RA. Structure of the actin-myosin complex and its implications for muscle contraction. Science. 1993; 261(5117): 58–65. [PubMed: 8316858]

Reyes A, He J, Mao CC, Bailey LJ, Di Re M, Sembongi H, Kazak L, Dzionek K, Holmes JB, Cluett TJ, et al. Actin and myosin contribute to mammalian mitochondrial DNA maintenance. Nucleic Acids Res. 2011; 39(12):5098–108. [PubMed: 21398640]

Rosenfeld SS, Xing J, Whitaker M, Cheung HC, Brown F, Wells A, Milligan RA, Sweeney HL. Kinetic and spectroscopic evidence for three actomyosin:ADP states in smooth muscle. J Biol Chem. 2000; 275(33):25418–26. [PubMed: 10827085]

Self T, Mahony M, Fleming J, Walsh J, Brown SD, Steel KP. Shaker-1 mutations reveal roles for myosin VIIA in both development and function of cochlear hair cells. Development. 1998; 125(4): 557–66. [PubMed: 9435277]

Self T, Sobe T, Copeland NG, Jenkins NA, Avraham KB, Steel KP. Role of myosin VI in the differentiation of cochlear hair cells. Dev Biol. 1999; 214(2):331–41. [PubMed: 10525338]

Smith CA, Rayment I. Active site comparisons highlight structural similarities between myosin and other P-loop proteins. Biophys J. 1996; 70(4):1590–602. [PubMed: 8785318]

Starr DA, Han M. Role of ANC-1 in tethering nuclei to the actin cytoskeleton. Science. 2002; 298(5592):406–9. [PubMed: 12169658]

Tyska MJ, Mackey AT, Huang JD, Copeland NG, Jenkins NA, Mooseker MS. Myosin-1a is critical for normal brush border structure and composition. Mol Biol Cell. 2005; 16(5):2443–57. [PubMed: 15758024]

Uyeda TQ, Kron SJ, Spudich JA. Myosin step size. Estimation from slow sliding movement of actin over low densities of heavy meromyosin. J Mol Biol. 1990; 214(3):699–710. [PubMed: 2143785]

Wang ZY, Wang F, Sellers JR, Korn ED, Hammer JA. Analysis of the regulatory phosphorylation site in Acanthamoeba myosin IC by using site-directed mutagenesis. Proceedings of the National Academy of Sciences. 1998; 95(26):15200–15205.

Wang Z, Edwards JG, Riley N, Provance DW Jr, Karcher R, Li Xd, Davison IG, Ikebe M, Mercer JA, Kauer JA, et al. Myosin Vb Mobilizes Recycling Endosomes and AMPA Receptors for Postsynaptic Plasticity. Cell. 2008; 135(3):535–548. [PubMed: 18984164]

Yang Y, Kovacs M, Sakamoto T, Zhang F, Kiehart DP, Sellers JR. Dimerized Drosophila myosin VIIa: a processive motor. Proc Natl Acad Sci U S A. 2006; 103(15):5746–51. [PubMed: 16585515]

Yengo CM, De la Cruz EM, Safer D, Ostap EM, Sweeney HL. Kinetic characterization of the weak binding states of myosin V. Biochemistry. 2002; 41(26):8508–17. [PubMed: 12081502]

Yengo CM, Sweeney HL. Functional role of loop 2 in myosin V. Biochemistry. 2004; 43(9):2605–12. [PubMed: 14992598]

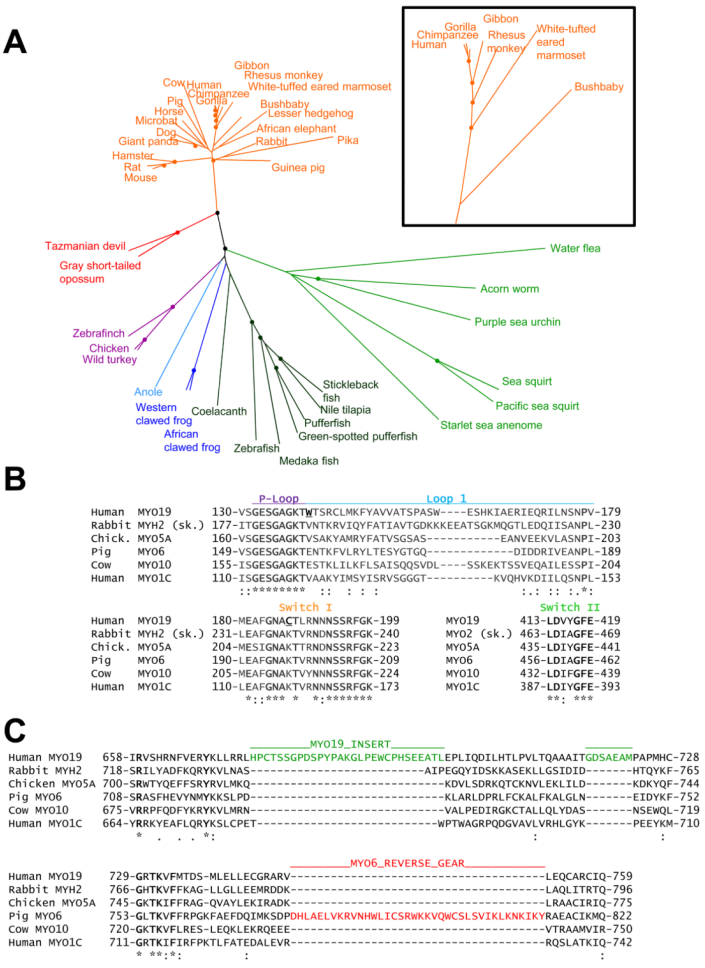

Figure 1. Myosin XIX orthologs have been identified in many species and exhibit conserved differences compared to other myosins

(A) An unrooted phylogenetic tree of 42 Myo19 orthologs from invertebrates (light green), fish (dark green), amphibians (dark blue), reptiles (cyan), birds (purple), and mammals (orange). Dots represent nodes validated by bootstrapping values of greater than 90%. (B) Comparisons of key catalytic regions within the motor domain of human MYO19 and other well-characterized myosins. Underlines indicate amino acids which are well-conserved across MYO19 orthologs but represent unique sequence differences when compared to other myosin classes. (C) Alignment of the converter domains of human MYO19 and other well-characterized myosins indicates MYO19-specific sequence insertions within the converter that do not correspond to the MYO6 “reverse gear” sequence insertion that reorients the lever-arm.

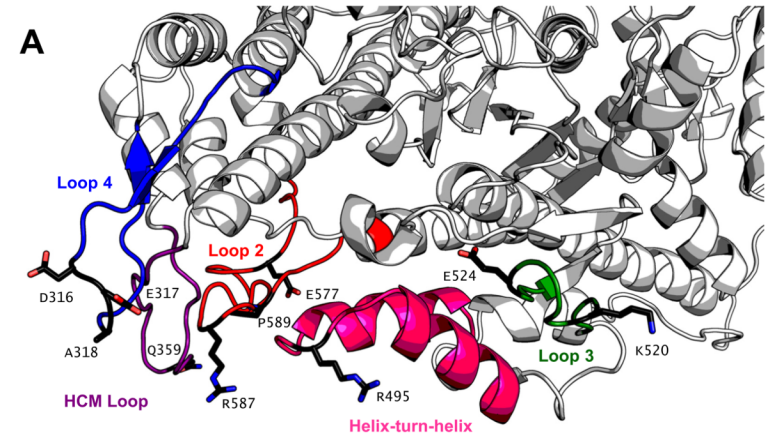

Phyre2 model of the MYO19 actin-binding interface

B

Loop 4		Charge
MYO19	307-GNIQFAASEDEAQPCQPMD-325	-4(-4)
MYH2(sk.)	363-GNMKFKQKQREE----QAE-377	+1
MYO5A	335-GNVEFASRDSDSCAIPPKH-353	-1
MYO6	348-GNIDFEEAGSTSGGCNLKN-366	-2
MYO10	337-GNIEFITAGG------AQV-349	-1
MYO1C	286-GNISFKEVGN-----YAAV-299	-1

Helix-turn-helix		Charge
MYO19	481-ISICSLINEECRLNRPSSAAQLQTRIET-508	0(0)
MYH2(sk.)	531-MGIFSILEEECMFPKATDTSFKNKLYDQ-558	-3
MYO5A	502-MGVLDLLDEECKMPKGSDDIWAQKLYNT-537	-3
MYO6	524-VGILDILDEENRLPQPSDQHFTSAGHQK-551	-3
MYO10	500-LGLLALINEESHFPQATDSTLLEKLHNQ-527	-3
MYO1C	457-PGIMSILDDVCATMHAVGEGADQTLLQK-484	-3

HCM Loop		Charge
MYO19	352-RTIRAGRQ--Q-QVFRKPC-367	+5(+5)
MYH2(sk.)	405-PRVKVGN-----EFVTKGQ-418	+2
MYO5A	376-RKLAT-----ATETYIKPI-390	+2
MYO6	394-RVMLTTAGGAKATVIKVPL-412	+3
MYO10	376-RSMFLRG-----EEILTPL-389	0
MYO1C	326-RQMDSKWGGKS-ESIHVTL-343	+1

Loop 3		Charge
MYO19	517-GHNKLSRE--------PSF-527	+1(+1)
MYH2(sk.)	567-QKPKVVKGKVE-----AHF-580	+3
MYO5A	538-EKPRLSN---------KAF-547	+2
MYO6	559-IPRKSKLAIHRNIAYDEGF-578	+2
MYO10	535-KPRVAVN---------NF-544	+2
MYO1C	493-EHFNSWN---------QGF-502	-1

Loop 2		Charge
MYO19	571-FPTN----------PKEKTQEEPPGQSRAPVLTVV-595	0(0)
MYO2(sk.)	624-FSGAQTAEAG----------NAQNGGAKKGGKKKGSSFQTVS-655	+4
MYO5A	591-LFQDEEKAISPTSATPSGRVPLSRTPVKPAKARPGQTSKEHKKTVG-636	+5
MYO6	622-FESSTN----------NNKDTKQKAGKLSFISVG-645	+2
MYO10	588-FEHVS----------SRNNQDTLKCGSKHRRPTVS-612	+3
MYO1C	546-FPEN----------LQADKKGRPTTAG-562	+1

Figure 2. Alignment of the sequences involved in actin interactions suggests differences in actin affinity

(A) The residues likely involved in acto-MYO19 interactions were determined by threading the human MYO19 sequence to a model of actin-bound MYH2 [Lorenz and Holmes 2010] using Phyre2 [Kelley and Sternberg 2009]. Residues at 8 out of 13 predicted electrostatic interactions between MYH2 and the actin filament are conserved in MYO19, but there is less conservation in the residues thought to make hydrogen bonds with actin. (B) Sequences thought to be involved in actin/MYO19 interactions show some variations in overall charge and amino acid makeup when compared to the corresponding sequences in other classified myosins. The net charge of zero for loop 2 and the separation of lysine residues by a negative charge could indicate an altered affinity for actin. However, the HCM loop carries a much higher positive charge than for other myosins, ranging from +3 to +6 in MYO19 orthologs analyzed. Similarly, the helix-turn-helix for Myo19 carries no charge, but it is negatively charged in other myosins (37/41 MYO19 orthologs contain a helix-turn-helix with a charge of 0 or greater). Blue indicates + charge, red indicates - charge, and bold indicates a perfectly conserved amino acid. The net charge for human MYO19 is indicated. The number in parentheses is the median charge for the 41 orthologs analyzed. Amino acids identified in [Lorenz and Holmes 2010] as forming electrostatic interactions with actin that are shown on the model are also underlined in the sequences. Asterisks (*) indicate positions which have a conserved residue, colons (:) indicate conservation between groups of strongly similar properties, and periods (.) indicate conservation between groups of weakly similar properties.

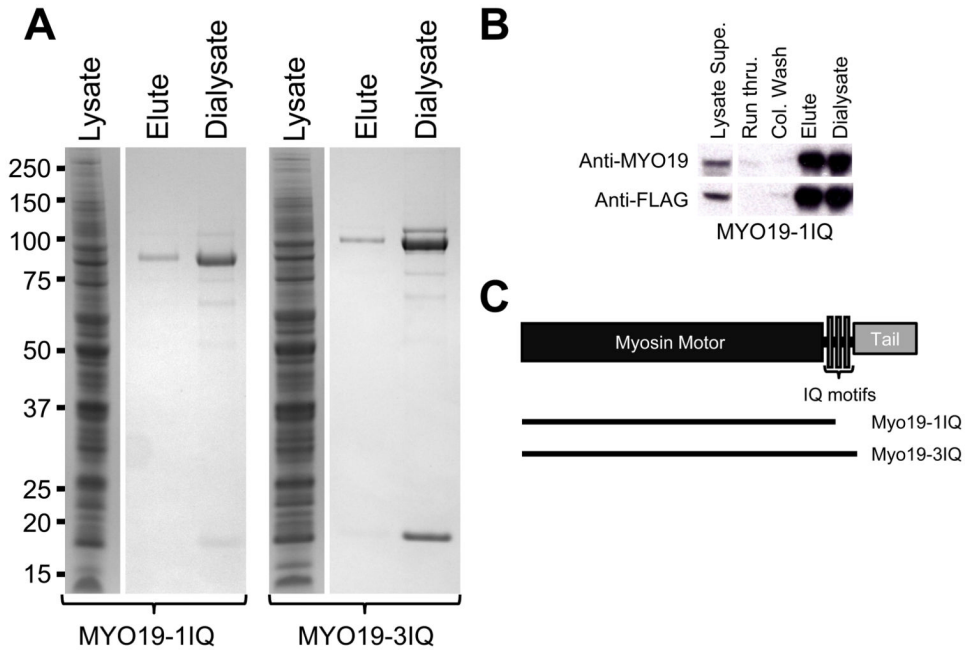

Figure 3. Truncations of human MYO19 can be expressed and purified from an insect-cell expression system

(A) FLAG-tagged MYO19-1IQ or MYO19-3IQ expressed in Sf9 cells can be affinity purified to high purity as seen by Coomassie-stained SDS-PAGE. (B) Both crude lysates and enriched fractions are reactive to antibodies against the FLAG-tag or MYO19, while washes show little reactivity to the antibodies as visualized via western blot. (C) A schematic representation of the domains included in the MYO19-1IQ and MYO19-3IQ constructs.

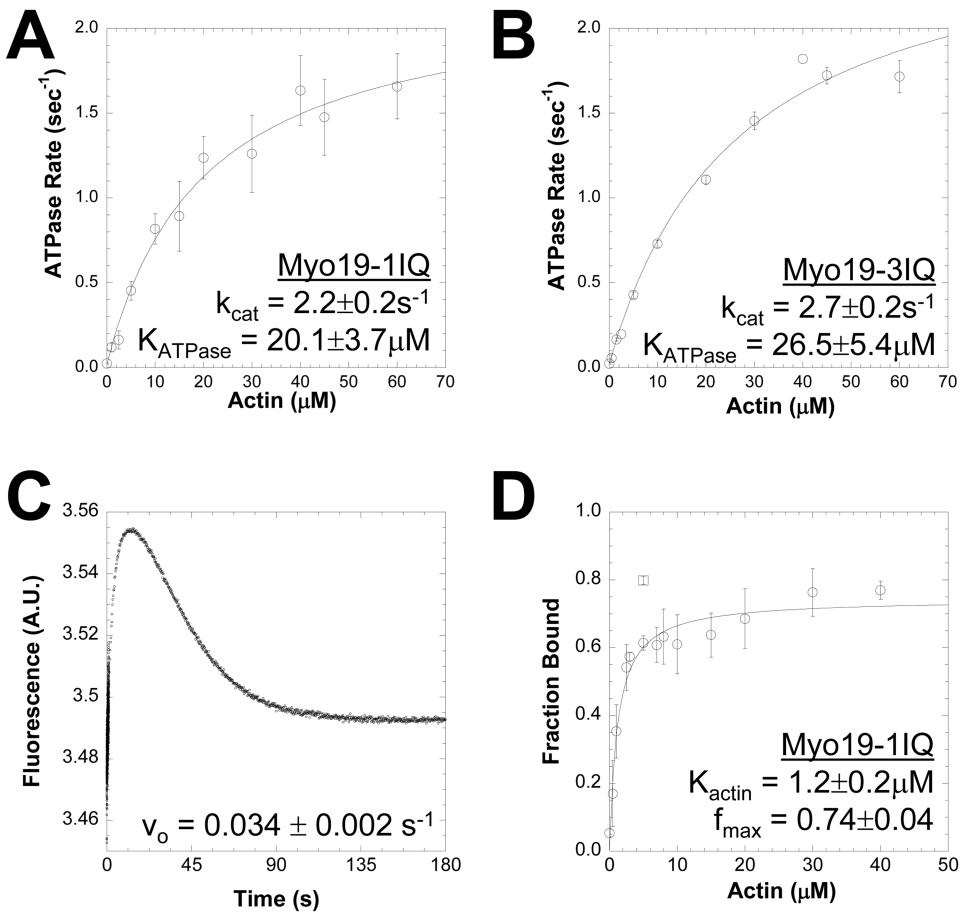

Figure 4. Steady-state enzymatic analysis of expressed MYO19 constructs indicate that it is an actin-activated ATPase

(A) Steady-state ATPase assays indicate that the Myo19-1IQ ATPase is activated by increasing actin concentration, a hallmark of myosin motors. Data are an average of 4-5 separate protein preparations. (B) Similar results were obtained with the Myo19-3IQ construct. Data are an average of 3-4 separate protein preparations. (C)Mixing of 0.25μM MantATP with 0.5μM Myo19-1IQ allows an estimate of v_o ~0.03 $ATPs^{-1}$ by fitting the fluorescence decay to a single exponential. (D)The affinity of Myo19-1IQ (0.5μM) for F-actin in the presence of 2mM ATP was measured by cosedimentation assay and quantified by densitometry of Coomassie-stained SDS-PAGE gels. Fraction bound is equal to the pellet fraction divided by the sum of the supernatant and pellet fractions. The □ represents the fraction of Myo19-1IQ bound to 5μM actin in the absence of ATP. Data are an average of 3 separate preparations. For A, B, and D, error bars represent SEM and errors for kinetic measurements are standard error of the fit.

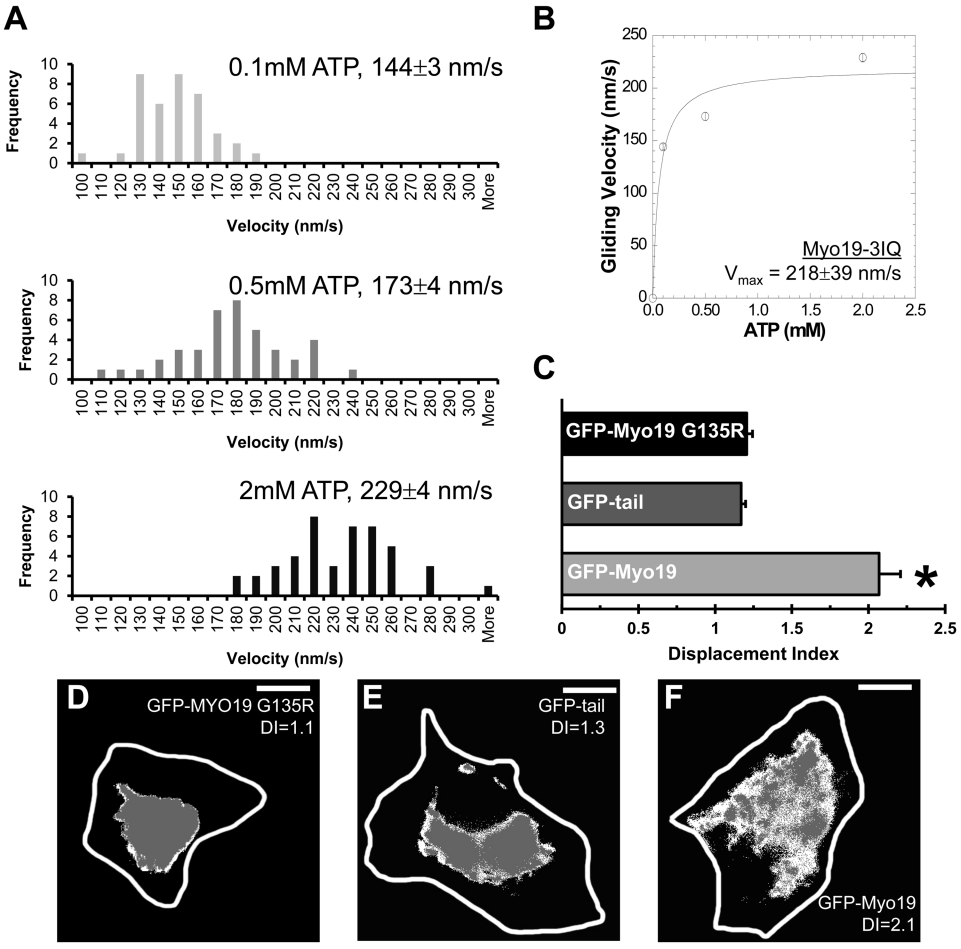

Figure 5. MYO19 is capable of inducing actin-based movement

(A) Purified Myo19-3IQ was adhered to nitrocellulose-coated coverslips using a chicken anti-human Myo19 antibody raised against the Myo19 tail. Rhodamine-phalloidin labeled actin filaments were added to the chamber, followed by the appropriate concentration of ATP. Time-lapse images were collected (1 frame/2 seconds, 2 minutes total time), and velocities calculated from the time-lapse movies using MtrackJ. (B) V_{max} was calculated by fitting the data to a hyberbola and assuming velocity = 0 at 0mM ATP. Data are mean plus or minus SEM, $n_{0.1mMATP}$=39 filaments, $n_{0.5mMATP}$=41 filaments, n_{2mMATP}=45 filaments across three different protein preps. Buffer conditions: 50mM KCl, 2mM $MgCl_2$, 1mM EGTA, 2mM DTT, 10mM imidazole, 0.7% methylcellulose, pH 7.0, 25°C. (C)Displacement index (DI) of the mitochondrial network was measured in A549 cells expressing GFP-MYO19 constructs. DI measures the dynamics of a set of objects by dividing the area containing those objects at the start of a time-lapse (gray) by the maximum projection. The maximum projection represents the space through which the objects moved during the time-lapse (white including grey). Only ectopic expression of full-length GFP-MYO19 resulted in an increased DI, while expression of GFP-MYO19G135R, which contains a motor-inactivating mutation, and GFP-MYO19 tail did not. Time-lapses were 3 minutes and 20 seconds in duration (*$p<0.05$ compared to other conditions, Tukey analysis). Error bars indicate SEM, n_{MYO19} = 28, n_{tail} = 11, and n_{G135R} = 8.Panels D-F are images representative of the data. The cell periphery is outlined in white. Scale bar = 10 μm.

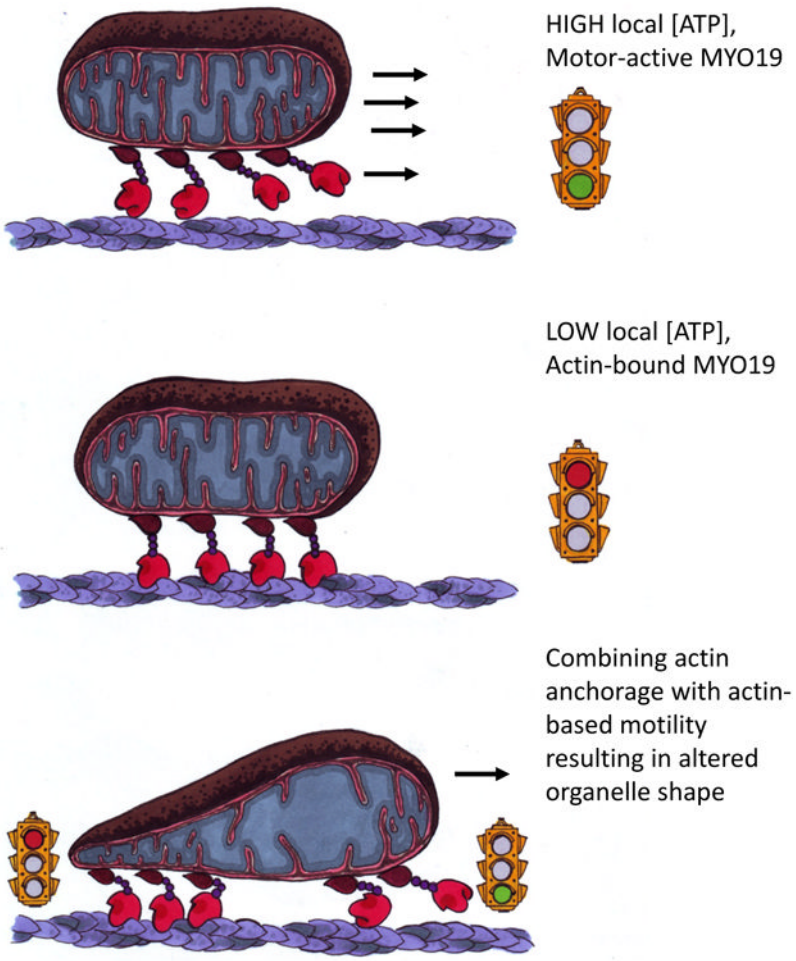

Figure 6. Possible roles for MYO19 in mitochondrial dynamics

The presence of a high duty ratio myosin motor on mitochondria suggests a number of possible roles for MYO19 in mitochondrial dynamics. Under conditions where local ATP concentrations are high, the mitochondria might relocate via a MYO19-powered mechanism. Upon reaching some critically low concentration of ATP, MYO19 may mediate binding between mitochondria and local actin, placing the organelle where ATP demands might be high. MYO19 may also serve to influence mitochondrial network shape and geometry through linkages to the actin cytoskeleton.

Table I
Well-conserved, charged amino acid residues located in the MYO19 actin-binding region

Human sequence number	Human MYO19 sequence	Motif	Comment
315-317	EDE	Loop 4	At least 2 negatively charged residues in all species except *Daphnia* and cow
352	R	HCM Loop	100% conserved across all aligned
359-361	QQQ	HCM Loop	At least 1 Q in all vertebrates. 2 Q in mammal, marsupial, bird, amphibian, and reptile
364-365	RK	HCM Loop	R or K at 364 in bird, reptile, marsupial, and mammal except rat, mouse, pig, cow, pika, and marmoset. R or K at 365 across all aligned
489-490	EE	Helix-turn-helix	100% conserved across all aligned
492	R	Helix-turn-helix	Conserved across all aligned except *Daphnia*
495	R	Helix-turn-helix	100% conserved across all aligned
505	R	Helix-turn-helix	R or K in all aligned
507	R	Helix-turn-helix	100% conserved in vertebrates
521	K	Loop 3	100% conserved in vertebrates
524-525	RE	Loop 3	R or K at 524 in vertebrates. E at 525 in mammal, marsupial, and reptile, except Tasmanian devil
577-578	EK	Loop 2	E at 577 in mammal and marsupial except hedgehog. K at 578 in in mammal and marsupial except hedgehog and dog.
581-582	EE	Loop 2	Conserved in mammal and marsupial except dog, opossum, and Tasmanian devil
588	R	Loop 2	R or K in amphibian, bird, reptile, marsupial, and mammal except turkey

MYO19 coding regions were trimmed down to the core motor domain, and then aligned using Clustal with the default settings [Larkin et al. 2007]. The loops involved in actin-binding were identified through a combination of alignment comparisons and comparison to threaded MYO19 models (see Figure 2). Particular charged residues were well-conserved within the actin-binding region across MYO19 orthologs, as noted in the “Comment” column.